Attosecond-Resolved Evolution of a Laser-Dressed Helium Atom: Interfering Excitation Paths and Quantum Phases

Niranjan Shivaram,[1,*] Henry Timmers,[1] Xiao-Min Tong,[2] and Arvinder Sandhu[1,†]

[1]*Department of Physics, University of Arizona, Tucson, Arizona 85721, USA*
[2]*Center for Computational Sciences, University of Tsukuba, Ibaraki 305-8573, Japan*

Using high-order harmonic attosecond pulse trains, we investigate the photoionization dynamics and transient electronic structure of a helium atom in the presence of moderately strong ($\sim 10^{12}$ W cm^{-2}) femtosecond laser pulses. We observe quantum interferences between photoexcitation paths from the ground state to different laser-dressed Floquet state components. As the intensity ramps on femtosecond time scales, we observe switching between ionization channels mediated by different atomic resonances. Using precision measurements of ion yields and photoelectron distributions, the quantum phase difference between interfering paths is extracted for each ionization channel and compared with simulations. Our results elucidate photoionization mechanisms in strong fields and open the doors for photoabsorption or photoionization control schemes.

Recent advances in "attosecond science" have given a new impetus to the study of atomic and molecular phenomena by providing direct real-time access to electron dynamics [1]. Experiments in this regime are typically conducted using extreme ultraviolet (XUV) attosecond pulses or pulse trains along with precisely synchronized strong-field femtosecond near-infrared (IR) laser pulses to obtain new insights into the dynamics of electronically excited systems [1–4]. As the roots of attosecond science lie in the strong-field concepts developed in the 1990s [5], the application of new attosecond techniques to refine our understanding of atomic or molecular dynamics in strong fields is of particular interest.

Using XUV attosecond pulse trains (APTs) and near-IR laser fields, we obtain precision real-time measurements of the transient nonequilibrium electronic structure of helium in intense fields. We investigate quantum interferences in the high-order harmonic driven photoexcitation paths to different components of a Floquet state. As the field intensity ramps on femtosecond time scales, we observe switching between different resonance-mediated ionization channels. We find that the ion yield from each ionization channel oscillates with a specific phase, which is determined by the quantum phase difference between transition matrix elements. We interpret this quantum phase using the Floquet interaction model. Numerical time-dependent Schrödinger equation (TDSE) calculations serve to elucidate the important role of Floquet interferences in photoexcitation and ionization.

We use amplified 65 fs, 785 nm IR pulses of 1.5 mJ energy, which are split into two parts. One part is focused onto a Xe-gas-filled hollow waveguide to generate an APT of high-order harmonics (HH). The APT, along with the copropagating driving infrared pulse (IR$_d$), is focused onto a He gas jet using a toroidal mirror. The second part, a

probe pulse (IR$_p$), goes to a delay stage and is focused on the He target with a 50 cm lens. The use of two IR fields (IR$_p$ and IR$_d$) is important in our measurements, as discussed later. The schematic of our experimental setup is provided in [6]. Photoelectrons are imaged using a velocity-map-imaging setup. He$^+$ ions are spatially imaged such that there is a one-to-one correspondence between the point of origin and the point at which they hit the detector, allowing us to eliminate Gouy phase averaging and obtain a high-quality signal [6].

Figure 1(a) schematically shows the experimental HH spectra relative to the unperturbed He resonances. The 15th harmonic is resonant with the $5p$ electronic state, and the 13th harmonic is slightly below the $2p$ resonance. Two other harmonics that we observe, i.e., the 11th and the 17th,
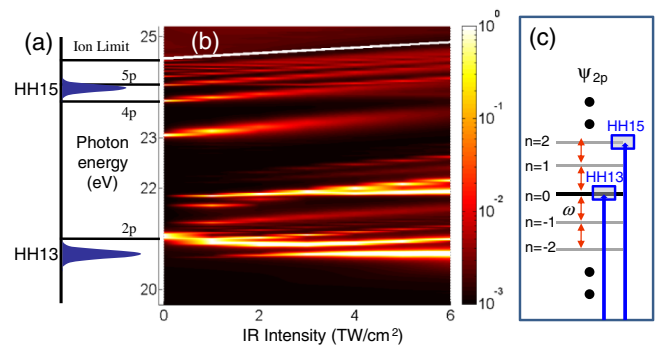

FIG. 1 (color online). (a) XUV spectrum and the relevant He states. (b) Calculated XUV photoabsorption cross section (in atomic units) as a function of laser intensity. (c) Floquet manifold showing one-photon-spaced components of the laser-dressed $2p$ state. The 13th and 15th harmonic excitation paths to $n = 0$ and $n = 2$ Fourier components are also shown. The interference between these two paths leads to 2ω oscillation.

are much weaker (20 times lower) and nonresonant. Hence, they do not play a significant role in this study. In Fig. 1(b), we show the photoabsorption cross section of He as a function of photon energy and peak IR intensity calculated using the method described in [7]. Clearly, the discrete atomic resonances evolve into a complicated structure even in a moderately intense laser field of the order of a few TW cm^{-2}. The higher excited states ($3p$, $4p$, $5p$, etc.) exhibit positive shifts, which can be approximated by the ponderomotive effect. The low-lying $2p$ state exhibits a negative shift and develops multiple branches. At intensities around 5 TW cm^{-2}, the excited state structure bears very little resemblance to the unperturbed case.

The physics of two-color photoionization dynamics is quite rich, even in a simple system like He, and multiple studies have recently focused on different facets of this topic [8–11]. In previous experiments with APT and IR fields, it has been observed that the He$^+$ ion yield oscillates as a function of time delay with half-IR-cycle periodicity [12,13]. This has been interpreted as an interference between wave packets generated by successive bursts in the APT [10,12,14]. Here, we explain the mechanisms underlying this interference process using the Floquet interaction picture [15]. Figure 1(c) shows the Floquet manifold corresponding to a laser-dressed atomic state (e.g., a $2p$ state), where different Fourier components are spaced by one IR-photon energy, i.e., ω. The Floquet manifold associated with an atomic state can be written as [15–17]

$$\psi_\alpha(t) = e^{-i\epsilon_\alpha t}\sum_n \phi_{\alpha n}e^{-in\omega t}, \qquad (1)$$

where ϵ_α is the quasienergy of the Floquet state and $\phi_{\alpha n}$ is the wave function of the nth Fourier component of this Floquet state. The two harmonics used in our experiment cause transitions to the $n = 0$ and $n = 2$ (or $n = -2$) components of the Floquet manifold, and the interference between these two paths modulates the excitation probability at the 2ω frequency [16,17]. The ionization probability, which is proportional to the excitation probability, thus exhibits an oscillatory variation at 2ω or half-cycle periodicity with time delay, which can be written as

$$P(\tau) \propto |M_0 f_0 + M_2 f_2 e^{-i(2\omega\tau+\phi)}|^2, \qquad (2)$$

where M_0 and M_2 are the transition matrix elements for the excitation to direct and two-photon-dressed Fourier components [e.g., $n = 0$ and $n = 2$ in Fig. 1(c)] and f_0 and f_2 are the corresponding strengths of the two harmonics. This formalism explains the origin of ion and electron yield oscillations and also provides an avenue to obtain quantitative information about the quantum phase ϕ between two paths. In this Letter, we demonstrate a method that allows a precise measurement of this quantum phase difference. Furthermore, we establish that this quantum phase changes as ionization channels switch dynamically with laser intensity. Thus, in contrast to prior studies which have

measured the phase of a resonance-mediated two-photon transition [8] or obtained the scattering phase shifts of continuum electron waves [11], our measurements focus on the intrinsic phase relationship between transitions to different components of a single laser-dressed state and its influence on the ionization dynamics. Importantly, this quantum phase difference determines the conditions for constructive or destructive interference in multipath ionization or fragmentation processes.

The quantum phase difference between excitation paths manifests itself in the form of a phase lag of the ion-yield oscillations. In order to accurately measure the intensity- or time-dependent phase lags, we need a reference signal. Below, we show that such a reference signal can be obtained using 2IR pulses. The net IR field in our experiment results from a combination of a weak pulse (IR$_d$) that is phase-locked to and copropagates with the APT and a strong pulse (IR$_p$) which is delayed relative to IR$_d$ by τ (Fig. 2). The delay dependence of the net IR intensity and phase is given as $I(\tau) = A_p^2 + A_d^2 + 2A_pA_d\cos(\omega\tau)$ and $\delta(\tau) = \arcsin[A_d\sin(\omega\tau)/\sqrt{I(\tau)}]$, where A_p and A_d are the amplitudes of the probe and driver IR fields. In the case of XUV + 2IR fields, the ionization probability given by Eq. (2) becomes

$$P(\tau) \propto |M_0 f_0 + M_2 f_2 e^{-i[2\omega\tau+2\delta_0-2\delta(\tau)+\phi]}|^2. \qquad (3)$$

The matrix elements now depend on the net IR intensity $I(\tau)$, which modulates at a frequency ω. δ_0 is the phase at which the attosecond pulse is locked to the driver IR field and is a constant in our experiment.

For a weak driver IR field ($A_d \ll A_p$), and considering the fact that the transition matrix element to a two-photon-dressed Fourier component, M_2, is at least an order of magnitude weaker than M_0 at our intensity parameters [7], it can be shown that the dominant frequencies in $P(\tau)$ are 1ω and 2ω. The ion yield $P(\tau)$ in the weak driver case can thus be written as

$$P(\tau) = T_1 \cos(\omega\tau) + T_2 \cos(2\omega\tau + 2\delta_0 + \phi), \qquad (4)$$

where T_1 and T_2 are delay-dependent amplitude factors. The next-order correction does not involve the 2ω frequency and is more than an order of magnitude smaller. It should be noted that the phase ϕ, which we are interested
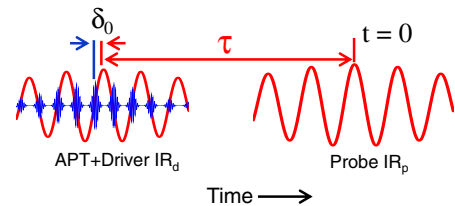

FIG. 2 (color online). The configuration of laser pulses used in the experiment. Time delay (τ) is negative when the probe IR$_p$ arrives earlier than the APT + driver IR$_d$ pulses. The APT is phase-locked to the driver IR at a phase of δ_0.

in measuring, does not appear in the 1ω term in Eq. (4). Hence, we can use the 1ω oscillations as a reference to measure the phase of 2ω oscillations.

Figure 3(a) shows the normalized experimental He^+ ion yield as a function of time delay between $APT + IR_d$ and probe IR_p for a probe IR intensity of $3.4\ TW\,cm^{-2}$. The driver IR intensity is less than $10^{10}\ W\,cm^{-2}$. The negative time-delay axis implies that the IR probe arrives ahead of the XUV pulse. As the time delay changes from -20 optical cycles towards zero, we observe a distinct oscillation structure with one-cycle and half-cycle components in accordance with Eq. (4). This asymmetric oscillation structure evolves from a high-left-peak structure to a high-right-peak structure as a function of the time delay. The change in oscillation structure is a direct manifestation of the change in phase relationship between the 2ω and 1ω components. This represents an intensity-dependent change in the phase of 2ω oscillations, which in turn implies that the quantum phase difference between the two interfering paths [ϕ in Eqs. (2) or (4)] is dependent on intensity conditions. The oscillation at the 1ω frequency, which arises from the intensity modulation due to the IR-IR interference, acts as a reference with respect to which we can robustly measure this phase ϕ by allowing us to compensate for interferometric drifts and other variations in our experiment.

Figure 3(b) shows the Fourier transform of the raw ion-yield oscillation signal over a time-delay range that spans more than 20 optical cycles. It is clearly seen that the spectrum contains only 1ω and 2ω frequencies, which is in agreement with Eq. (4).

Before we quantitatively discuss the variation of the interference phase ϕ with intensity, it is important to identify the different Floquet states contributing to the ionization. To identify the Floquet paths, we utilize photo-electron spectroscopy. Figure 4(a) shows the experimental electron spectra at different probe intensities. The observed electron peaks in Fig. 4(a) are associated with IR ionization of XUV excited $5p$, $4p$, and $2p$ atomic states. At low intensities, ionization is mediated by the $5p$ resonance, and we observe a strong peak corresponding to the $5p + 1\omega$ process. This is expected, as the 15th harmonic is initially resonant with the $5p$ state. As the intensity is increased, the $4p + 1\omega$ channel starts contributing. At higher intensities, the $2p + 3\omega$ channel dominates the ionization signal. TDSE calculations for comparable intensity parameters yield similar results [Fig. 4(b)]. The experimental angle-resolved photoelectron images in Fig. 4(c) also show that, as intensity is increased towards $3.4\ TW\,cm^{-2}$, side lobes corresponding to the "g-wave" structure appear. This is another indication of the three-photon ionization of the XUV excited $2p$ state. These observations are in good agreement with Fig. 1(b) as the $2p$ structure Stark shifts downward in energy with increasing intensity, becoming resonant at
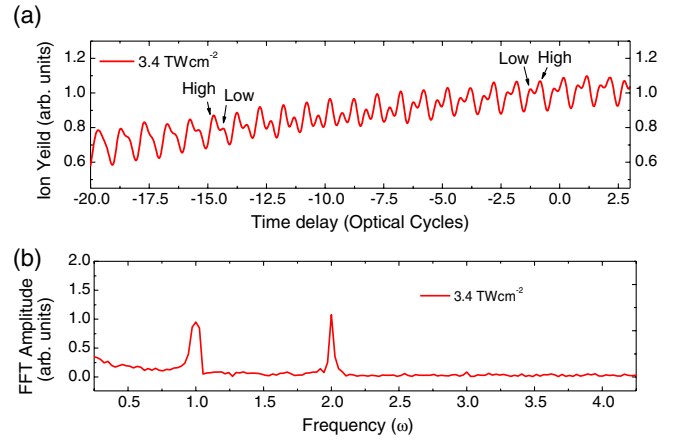

FIG. 3 (color online). (a) Normalized He^+ ion-yield oscillations for XUV and 2IR pulses at a probe intensity of $3.4\ TW\,cm^{-2}$. Asymmetry in the double peak oscillation structure is indicative of the phase difference between the 1ω and 2ω frequencies. The asymmetry gets reversed as the time delay or instantaneous intensity is varied. (b) Fast Fourier transform (FFT) amplitude of the raw ion-yield oscillations shows only two prominent frequencies. As the noise floor at frequencies $>3\omega$ is insignificant, it has been subtracted from (a) to improve the clarity of the oscillation structure.

higher intensities. Thus, the results from Fig. 4 confirm that the dominant two-color ionization pathway changes from $5p$-mediated ionization at low intensities to $2p$-mediated ionization at higher intensities. Next, we extract the real-time variation of the interference phase ϕ and establish a quantitative relationship between the strong-field modification of atomic structure and the intensity-dependent phase change observed in the ion-yield oscillations of Fig. 3.

The extraction of the phase of the 2ω component of ion-yield oscillations relative to the 1ω component is
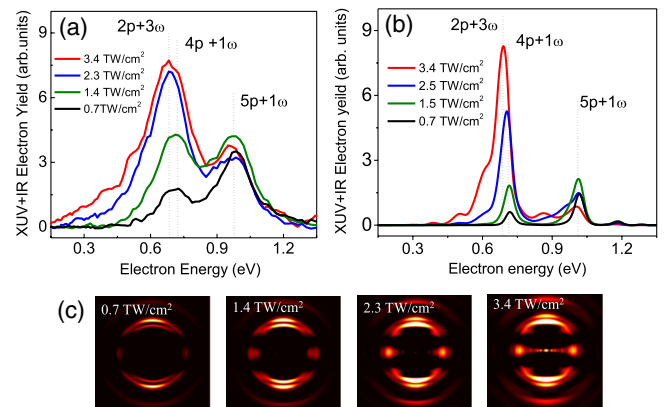

FIG. 4 (color online). (a) Experimental $XUV + IR_p$ photoelectron spectrum of He at different IR_p intensities. As the IR intensity is increased, the $2p + 3\omega$ peak becomes dominant. (b) Calculated photoelectron spectrum. (c) Experimental velocity map imaging of photoelectrons at different IR_p intensities.

performed using a Fourier-transform-based method [18]. The ion signal is first Fourier transformed to the frequency domain, and a rectangular window function is applied around the 2ω peak. This windowed peak is then translated to the zero frequency position, and the array is then inverse Fourier transformed back to the time-delay domain. The phase of the complex number array obtained gives the time-delay-dependent phase of the 2ω signal. This procedure is repeated for the 1ω peak, and the phase of the 1ω signal is used as a reference to obtain the phase of the 2ω signal free of interferometric drifts and fluctuations.

Figure 5(a) plots the phase ϕ as a function of time delay (solid line). In this plot, a constant phase offset corresponding to the APT timing δ_0 [Eq. (4)] has been removed by comparing our measurements with the TDSE simulations described below. Assuming a Gaussian profile, we calibrate the time-delay axis such that each delay value corresponds to a specific instantaneous intensity [top axis of Fig. 5(a)]. The right and left insets in Fig. 5(a) show independent experimental measurements of ion-yield oscillation at 3.4 TW cm^{-2} and 1.4 TW cm^{-2} peak intensities, respectively. The asymmetry of the double peak structure in the oscillation signal is opposite for the two intensities, consistent with the observations in the real-time
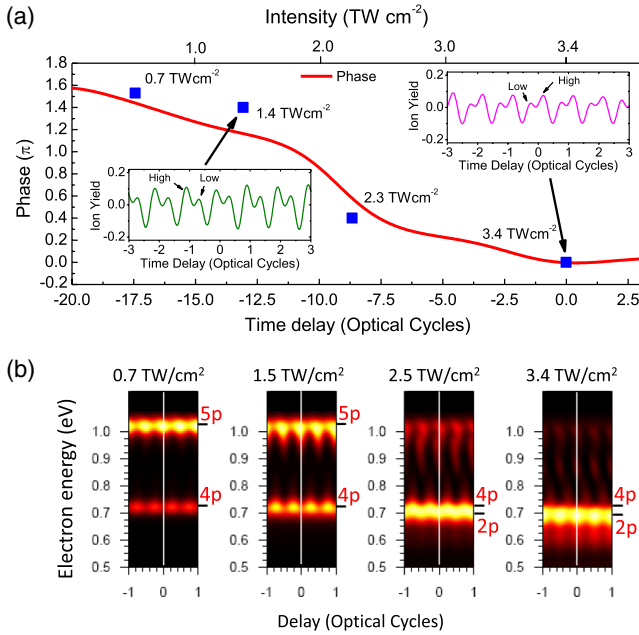

FIG. 5 (color online).   (a) The solid red curve shows the phase of the 2ω component of ion-yield oscillations with time delay for a probe intensity of 3.4 TW cm^{-2}. The blue squares represent independent phase measurements conducted at different peak intensities. The insets show the experimental ion-yield oscillations near zero time delay for two representative peak intensity values. The difference in oscillation structure provides independent verification of the phase change. (b) TDSE results showing the energy-resolved oscillations in the XUV + IR$_p$ electron yield of various resonance-mediated ionization channels.

variation in Fig. 3(a). We repeat the phase extraction exercise on ionization signals obtained at different peak intensities and obtain the phase of the 2ω component in each case. We then plot the phases extracted for different peak intensities as squares in Fig. 5(a) and compare them with the delay-dependent phase curve. A good match between the two independent results demonstrates the soundness of our experimental method.

Starting from zero, as we move to longer time delays (i.e., lower intensities), the experimentally obtained phase increases [Fig. 5(a)]. The experimental value of the phase goes through π and reaches 1.5π at 1.4 TW cm^{-2} intensity. This variation of phase can now be understood in terms of the quantum mechanical phases associated with various ionization channels and the relative dominance of different channels. The calculated energy-resolved XUV + IR$_p$ photoelectron data in Fig. 5(b) elucidate the role of the different channels. At high intensity (3.4 TW cm^{-2}), the $2p$ resonance-mediated ionization channel at 0.69 eV dominates. The oscillation of this channel has zero phase, implying that the ionization yield peaks at zero delay, where XUV bursts are synchronized to the peak of the IR field. For this to happen, the quantum phase ϕ between the M_0 and M_2 transition matrix elements in Eq. (2) has to be zero. In other words, 13HH and 15HH induced transitions to the Floquet components associated with $2p$ excitation [Fig. 1(c)] are "in-phase."

As intensity decreases, the $4p$ channel at 0.72 eV starts contributing substantially. Interestingly, the oscillations in this channel are completely out of phase with the $2p$ contribution [Fig. 5(b), 1.5 TW cm^{-2}]. This implies that $\phi = \pi$ for the $4p$-mediated ionization channel, and the ionization yield peaks when XUV bursts are synchronized to the zeros of the IR field. In the Floquet picture, the 13th and 15th HH transition matrix elements to the $n = -2$ and $n = 0$ components of the $4p$ Floquet state have opposite signs. In general, as the transition matrix elements to bound states are real, there are only two possibilities; either M_0 and M_2 can have the same sign ($\phi = 0, 2\pi$) or opposite signs ($\phi = \pi$), and we see both possibilities in Fig. 5(b). At very low intensity, the $5p$ ionization starts dominating and oscillates with the same phase as $2p$. This implies that the phase between the $n = -2$ and $n = 0$ components of $5p$ is 0, $\pm 2\pi$. Thus, in our experiment, as the intensity decreases or time delay gets longer, we observe in real time a change in the phase of ion-yield oscillation, going from zero when $2p$ is dominant, through π where $4p$ contributes substantially, and eventually towards 2π where $5p$ dominates.

Our work represents a direct measurement of the quantum phases associated with XUV + IR ionization channels, which are not known *a priori*. These observations are general and should be valid whenever XUV excitation occurs in a strong field. The Floquet-theory-based nonperturbative model gives crucial insight into these seemingly complex

processes and explains the mechanisms underlying quantum interferences in ionization. The measurement of switching between ionization paths and the accompanying quantum phases provides a framework on which we can build methods to control excitation and ionization dynamics in the presence of strong fields. For example, a strong field with appropriate intensity and timing can be used to control the interfering matrix elements and hence the yield and spectral content of photoelectrons emitted from an atom, a molecule, or a surface. A recent Letter [9] on XUV transparency in the presence of strong fields validates some of these ideas.

While our Letter only explores the role of quantum interferences and strong fields in atomic ionization, molecular excited states present a richer and more complex system. We expect the quantum interferences between Floquet transitions to play an important role in the control of molecular excitation and dissociation dynamics. For example, recent work [19] in H_2 invoked XUV + IR multi-path interferences for control of the dissociation process. The knowledge of transient atomic and molecular structure and the quantum phases of interfering pathways is thus crucial to understanding the dynamics and to devising new control strategies in attoscience, where XUV and strong fields are now being routinely used to study the behavior of matter on electronic time scales.

---

*niranjan@physics.arizona.edu

†sandhu@physics.arizona.edu

[1] F. Krausz and M. Ivanov, Rev. Mod. Phys. **81**, 163 (2009).

[2] J. Mauritsson, T. Remetter, M. Swoboda, K. Klunder, A. L'Huillier, K. J. Schafer, O. Ghafur, F. Kelkensberg, W. Siu, P. Johnsson, M. J. J. Vrakking, I. Znakovskaya, T. Uphues, S. Zherebtsov, M. F. Kling, F. Lepine, E. Benedetti, F. Ferrari, G. Sansone, and M. Nisoli, Phys. Rev. Lett. **105**, 053001 (2010).

[3] A. S. Sandhu, E. Gagnon, R. Santra, V. Sharma, W. Li, P. Ho, P. Ranitovic, C. L. Cocke, M. M. Murnane, and H. C. Kapteyn, Science **322**, 1081 (2008).

[4] S. Gilbertson, M. Chini, X. M. Feng, S. Khan, Y. Wu, and Z. H. Chang, Phys. Rev. Lett. **105**, 263003 (2010).

[5] P. B. Corkum, Phys. Rev. Lett. **71**, 1994 (1993).

[6] N. Shivaram, A. Roberts, L. Xu, and A. Sandhu, Opt. Lett. **35**, 3312 (2010).

[7] X. M. Tong and N. Toshima, Phys. Rev. A **81**, 063403 (2010).

[8] M. Swoboda, T. Fordell, K. Klunder, J. M. Dahlstrom, M. Miranda, C. Buth, K. J. Schafer, J. Mauritsson, A. L'Huillier, and M. Gisselbrecht, Phys. Rev. Lett. **104**, 103003 (2010).

[9] P. Ranitovic, X. M. Tong, C. W. Hogle, X. Zhou, Y. Liu, N. Toshima, M. M. Murnane, and H. C. Kapteyn, Phys. Rev. Lett. **106**, 193008 (2011).

[10] M. Holler, F. Schapper, L. Gallmann, and U. Keller, Phys. Rev. Lett. **106**, 123601 (2011).

[11] L. H. Haber, B. Doughty, and S. R. Leone, Phys. Rev. A **79**, 031401 (2009).

[12] P. Johnsson, J. Mauritsson, T. Remetter, A. L'Huillier, and K. J. Schafer, Phys. Rev. Lett. **99**, 233001 (2007).

[13] P. Ranitovic et al., New J. Phys. **12**, 013008 (2010).

[14] P. Riviere, O. Uhden, U. Saalmann, and J. M. Rost, New J. Phys. **11**, 053011 (2009).

[15] S. I. Chu and D. A. Telnov, Phys. Rep. **390**, 1 (2004).

[16] X. M. Tong, P. Ranitovic, C. L. Cocke, and N. Toshima, Phys. Rev. A **81**, 021404 (2010).

[17] X. M. Tong and N. Toshima, Phys. Rev. A **81**, 043429 (2010).

[18] M. Takeda, H. Ina, and S. Kobayashi, J. Opt. Soc. Am. **72**, 156 (1982).

[19] F. Kelkensberg, W. Siu, J. F. Perez-Torres, F. Morales, G. Gademann, A. Rouzee, P. Johnsson, M. Lucchini, F. Calegari, J. L. Sanz-Vicario, F. Martin, and M. J. J. Vrakking, Phys. Rev. Lett. **107**, 043002 (2011).